ChemCatChem

Research Article
doi.org/10.1002/cctc.202401794

Chemistry Europe
European Chemical Societies Publishing

www.chemcatchem.org

# The Influence of Reaction Conditions on Selective Acetylene Hydrogenation Over Sol Immobilization Prepared AgPd/$Al_2O_3$ Catalysts

Jake O. Williams,[a] Ella Kitching,[a] Rhea-Shree Patel,[a] Jonathan M. Mauß,[b] Klara S. Kley,[b] Rohini Khobragade,[b] Jacopo de Bellis,[b] David J. Morgan,[a] Thomas Slater,[a] Ferdi Schüth,[b] Stuart H. Taylor,[a] Nicholas F. Dummer,*[a] Michael Bender,[c] and Graham J. Hutchings*[a]

Electric plasma activation of methane opens up the possibility to produce ethene, an important platform chemical in industry, by using sustainable resources like biogas or hydrogenated carbon dioxide and electricity from renewable energies. The ethene stream of such pyrolysis plants contains much higher concentrations of acetylene (≥15 vol.%) compared to ethene from conventional steam cracking of naphtha (<2 vol.%). In this study, silver-palladium catalysts in various compositions supported on alumina were synthesized via a sol-immobilization technique and investigated in the selective gas-phase hydrogenation of equally concentrated acetylene-ethene mixtures under industrially relevant pressures. A molar Pd concentration of around 10 % in the PdAg alloyed nanoparticles was identified as the optimum composition for simultaneous high activity and ethene selectivity under catalysis conditions. Higher temperatures seem to be crucial for the stability of the catalysts on-stream most likely via increased desorption of active site blocking and high-boiling oligomers from acetylene. The best performing $Pd_{10}Ag_{90}$ displayed an ethene, ethane and $C_{4+}$ selectivity of 65%, 4%, and 14%, respectively, at 175 °C while being active for more than 200 min. The performance of the catalyst was compared with catalysts synthesized via a mechanochemical and a conventional wet-impregnation procedure.

## 1. Introduction

Ethene is extremely important to modern society due to its two main uses, the first and predominant application is the formation of polyethylene via polymerization. Second, ethene can be used as a C2 feedstock to synthesize important and high demand molecules such as ethylbenzene, polyethylene glycol (PEG) and polyvinylchloride (PVC).[1] Due to its importance, ethene is globally the most produced organic chemical with a production volume of 185 Mtons in 2018, increasing to 214.3 Mtons in 2021. It is forecast that the production of ethene will further increase by 7%–10% in the next 5 to 10 years.[2] Today, most of the ethene is produced via the steam cracking of different fossil feedstocks including ethane, naphtha, gas oil, and coal. The composition of the products depends on the initial feedstock but when ethane is used, 80% of the product stream is ethene and up to 2% is acetylene.[3] Whilst it would currently be a large transition away from steam cracking, diversifying how ethene is produced is pivotal for the future de-fossilization of the chemical industry focusing on more sustainable processes. The Hüls plasma reforming process represents a highly promising alternative to produce ethene from more sustainable feedstocks while benefitting from the use of renewable energies. In this process, ethene is formed through the use of an electric plasma arc to convert biogas, natural gas or biomass to a mixture of acetylene, ethene, hydrogen, and carbon black.[4] The acetylene (≥15 vol.%) in the effluent ethene streams are substantially higher compared to steam cracking of naphtha (<2 vol.%) which requires newly optimized catalysts for the selective gas-phase hydrogenation for downstream purification.[5] The presence of acetylene impurities in ethene streams is undesirable as acetylene poisons the catalyst used for the polymerization of ethene. The concentration of acetylene must therefore be lowered to <5 ppm to avoid poisoning.[5b,6]

Catalysts used for acetylene hydrogenation in ethene streams have two main considerations; they must be selective in producing ethene and not over-hydrogenating to ethane, and they must minimize oligomer formation from side-reactions.[4] The side reactions initially produce butadiene, however, longer

[a] J. O. Williams, E. Kitching, R.-S. Patel, D. J. Morgan, T. Slater, S. H. Taylor, N. F. Dummer, G. J. Hutchings
Max Planck- Cardiff Centre on the Fundamentals of Heterogeneous Catalysis FUNCAT, Cardiff Catalysis Institute, Translational Research Hub, Cardiff University, Maindy Road, Cardiff CF24 4HQ, UK
E-mail: dummernf@cardiff.ac.uk
hutch@cardiff.ac.uk

[b] J. M. Mauß, K. S. Kley, R. Khobragade, J. de Bellis, F. Schüth
Max-Planck-Institut für Kohlenforschung, Department of Heterogeneous Catalysis, Kaiser-Wilhelm-Platz 1, Mülheim an der Ruhr 45470, Germany

[c] M. Bender
BASF SE, RGU/CU–build. M301, Carl-Bosch-Strasse 38, Ludwigshafen am Rhein 67056, Germany

Supporting information for this article is available on the WWW under https://doi.org/10.1002/cctc.202401794

chains are formed when additional units of acetylene can react and bond. These side products are known as "green oil" and their formation is undesirable as it lowers the overall yield of ethene and poisons the catalyst surface. Due to the sheer scale of ethene production, partial hydrogenation of acetylene has been well studied both academically and industrially and many different catalyst systems have been reported so far. The most widely studied catalysts for selective acetylene hydrogenation are supported nanoparticles of palladium often with additive metals to improve the activity or the selectivity, these additives can include Cu,[7] Zn,[8] Ni,[9] Au,[10] and Ag.[11] Besides electronic effects, additive metals are believed to reduce palladium ensemble sizes and thereby weaken the adsorption of ethene on the catalyst surface favoring desorption over further hydrogenation to ethane.[12] The results of studies on the origin of oligomers formation are much more ambiguous and range from strong Pd—C bonds of acetylene, vinylidene and vinyl species on larger palladium clusters to local deficiencies of activated hydrogen species.[12,13]

The high exothermicity of the hydrogenation reaction and the increased oligomerization tendency at higher acetylene concentrations makes it particularly challenging for catalysts to become selective in the selective hydrogenation of acetylene-ethene mixtures after plasma reforming. Several groups are currently researching selective hydrogenation of equally concentrated acetylene-ethene mixtures. The Schüth group, for example, has developed a mechanochemically synthesized $Pd_1Ag_9/Al_2O_3$ catalyst that displays a selectivity to ethene of ca. 60% at 100 °C, and ca. 70 % at 150 °C, at 10 bar and full acetylene conversion under the above-mentioned feed composition.[4a] The selectivity to ethane and $C_4$ molecules was 10%–20 % and 10% at 100 °C, and 10% and 10% at 150 °C, respectively. While having a quite similar selectivity performance than conventionally wet-impregnated catalysts, the mechanochemically synthesized materials demonstrated an exceptionally high stability on-stream of more than 10 h. This lifetime advantage was attributed to the substantially higher surface area of the alumina support that slows down deactivation processes via the deposition of high-boiling acetylene oligomers. Recently, the same group has reported even higher ethylene selectivity of up to 82% and lifetimes of more than 20 h at 120 °C, 10 bar, and full acetylene conversion under those demanding reaction conditions by modifying the surface of non-selective palladium catalysts with selected ionic liquids. Those SCILL-type catalysts (solid catalyst with ionic liquid layer) clearly outperform bimetallic catalysts reported so far under those reaction conditions.[14]

Particle size, surface composition and ensemble sizes in multi-metallic nanoparticles influencing their behavior in catalysis are highly dependent on the way they have formed during synthesis. The predominant methods of catalyst synthesis are co-precipitation, impregnation, or deposition precipitation methods depending on the metal being deposited, the support and the amount of catalyst required. Catalyst preparation through sol immobilization typically yields small supported metal nanoparticles (2-5 nm) with a narrow size distribution for various supported metals such as Ru,[15] Pd,[16] Pt,[17] and Au.[18] The procedure has been expanded to the synthesis of bimetallic compounds like Pd-Pt[19] and Pd-Au[20] catalysts. Sol immobilization uses a polymer to stabilize metal nanoparticles within a sol, before the support is added and the sol is immobilized by in situ reduction to form the catalyst.

In this study we have used a sol immobilization technique to synthesize palladium-silver alloyed nanoparticles of different composition supported on alumina. To our knowledge this is the first reported example of this preparation with Ag-Pd. These catalysts were then investigated them in the selective hydrogenation of equally concentrated acetylene-ethene mixtures at industrially relevant high pressure. Current commercial catalysts for the selective gas-phase hydrogenation of acetylene impurities are not optimized with respect to consistent size and composition of Ag and Pd nanoparticles or for those harsh reaction conditions with respect to the high reaction exothermicity and increased oligomerization processes. The results reveal the importance of catalyst synthesis method to address alloy composition, nanoparticle size and reaction conditions for simultaneous high ethene selectivity and lifetime on-stream.

## 2. Results and Discussion

### 2.1. Catalyst Characterization

A sample of spherical (3–4 mm) alumina was gratefully provided by Saint–Gobain Norpro and when ground had a specific surface area of 54 $m^2\ g^{-1}$ (pore vol. 0.26 cc $g^{-1}$). The sample was powdered through grinding with an agate pestle and mortar and used as the metal nanoparticle support. Prior to metal deposition a powdered sample was examined by powder XRD to identify the phases present and the patterns underwent Rietveld refinement to characterize the lattice parameters of the crystalline phases. Refinement was carried out with the X'pert High Score Plus software using Crystallographic Information Files (CIF) that matched the identified phases. Figure S1 illustrates the refinement analysis, whereby the agreement profile or $R_{profile}$ was 5.14% ($R_{wp} = 7.04\%$ and $\chi^2 = 7.83$) of the mixed phase material (see Supplemental Information). Refinement indicated that the alumina was comprised of 80.6% $\alpha$-alumina (ICSD 73,725) and 19.4% $\theta$-alumina (ICSD 82,504). The space group of $\alpha$-alumina is 167, being hexagonal in structure ($R\bar{3}c$) with lattice parameters of a/$b$ = 4.7597 Å, $c$ = 12.9937 Å (alpha/beta = 90° and gamma = 120 °). The minor $\theta$-phase is monoclinic (beta), according to space group 12 (C2/m), with lattice parameters of $a$ = 11.797 Å, $b$ = 2.904 Å, $c$ = 5.623 Å, alpha/gamma = 90° and beta 103.9°. Following this, three alumina supported catalysts were synthesized via a sol-immobilization method, with Ag and modestly increasing Pd fractions (4.7%, 5.6%, and 10.1%). The catalysts were *ca*. 1 wt.% total metal loading, the actual values as measured from ICP-MS analysis are reported in Table 1.

TEM imaging of the three catalysts revealed that AgPd was present mainly in the form of isolated single nanoparticles (Figure 1). The size and morphology of nanoparticles did not greatly vary between the three different loadings, although smaller nanoparticles could be found on the sample with highest Pd loading ($Pd_{10}$). Further images and representative

**Table 1.** Metal loading and composition of the supported Ag-Pd/$\theta\alpha$-$Al_2O_3$ catalysts and specific surface area and pore volume.

| Catalyst | Total Metal Loading[a)] (wt.%) | Composition[a)] (%) | | Ag/Pd Ratio | SSA ($m^2$ $g^{-1}$) | Pore Vol. (cc $g^{-1}$) |
|---|---|---|---|---|---|---|
| | | *Pd* | *Ag* | | | |
| $Pd_5$ | 0.89 | 4.7 | 95.3 | 20 | 49 | 0.23 |
| $Pd_6$ | 1.01 | 5.6 | 94.4 | 17 | 41 | 0.21 |
| $Pd_{10}$ | 0.79 | 10.1 | 89.9 | 9 | 44 | 0.19 |

[a)] Loading and composition calculated from ICP-MS, samples dissolved in $HNO_3$.

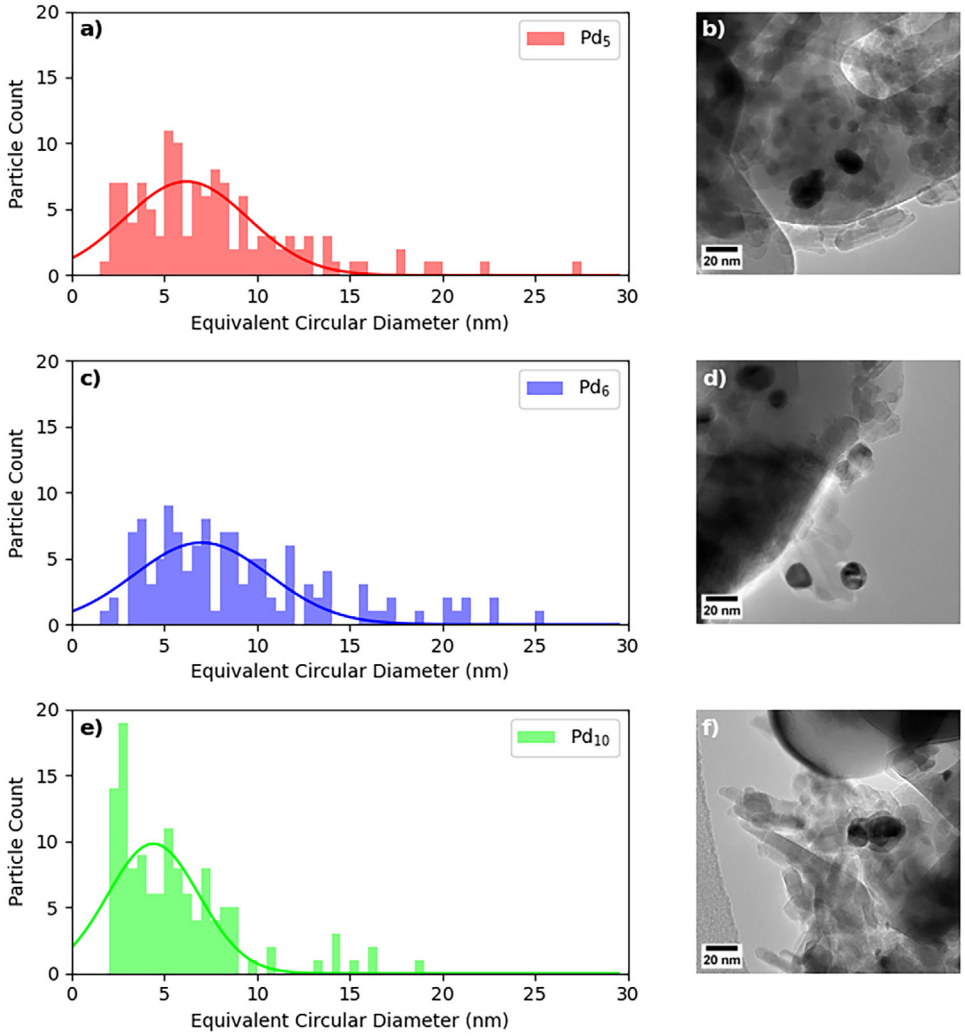


**Figure 1.** Particle size distributions (left) and representative bright field TEM images (right) of (a and b) $Pd_5$, (c and d) $Pd_6$, and (e and f) $Pd_{10}$. Further images of the catalysts are shown in Figure S2, including representative color segmentation analysis.

segmentation analysis to support the data in Figure 1 is displayed in Figure S2. Nanoparticles were consistently observed to be homogeneous alloys of Ag and Pd (see STEM-EDX elemental mapping in Figure 2).

The respective mean equivalent circular diameter (ECD) of $Pd_5$, $Pd_6$, and $Pd_{10}$ were 7.6 ± 4.4 nm, 8.9 ± 5.0 nm, and 5.6 ± 3.3 nm, respectively, as measured from sample sizes of >120 particles. Whilst the overall distribution is similar across the three samples, $Pd_{10}$ has a larger proportion of particles with <3 nm diameter.

XPS analysis of the PdAg samples revealed both Ag and Pd were present with the latter in lower concentration in line with ICP analysis the atomic concentrations are given in Table 2. It should be noted that given the low concentrations, the ratio will have some error, nevertheless the observed trend is comparable to that observed by ICP (Table 1). As such the Ag/Pd ratio from XPS analysis for the three catalysts agrees with the Ag/Pd ratios calculated from ICP except the $Pd_6$ catalyst, which exhibits a higher Ag content. As XPS is a surface sensitive technique, this may be a sign of surface enrichment by Ag in the alloyed

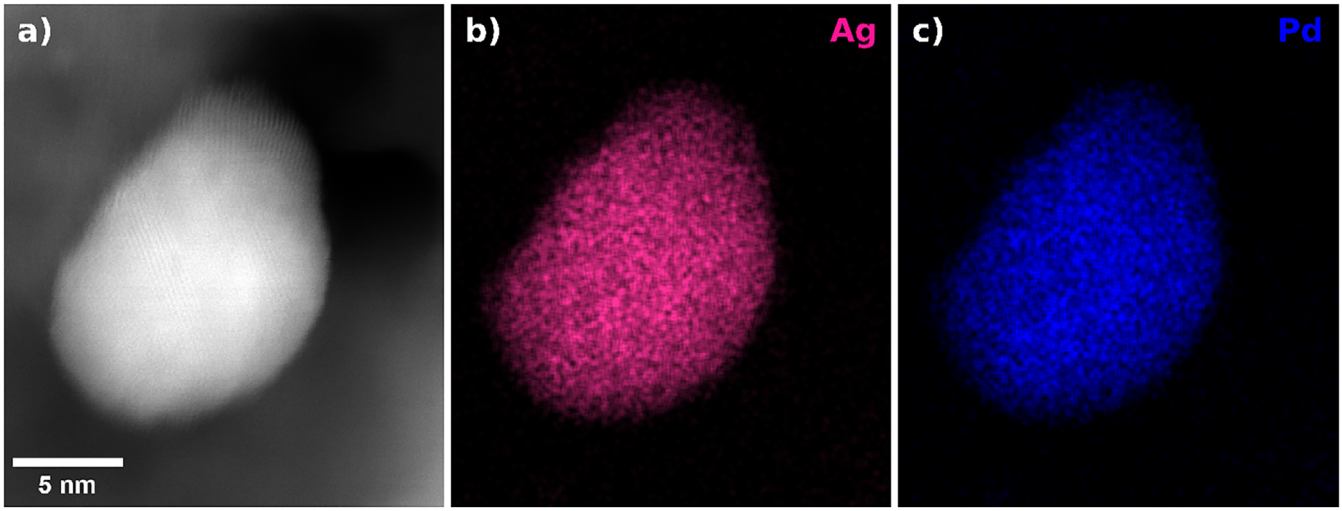


**Figure 2.** (a) HAADF–STEM image of single AgPd nanoparticle with associated STEM–EDX elemental maps of (b) Ag and (c) Pd. Ag and Pd were observed to be homogeneously distributed across all bimetallic nanoparticles.

**Table 2.** XPS derived homogeneous equivalent atomic concentrations (at.%).

| Sample | Concentration (at.%) | | | | | Ag/Pd Ratio |
|---|---|---|---|---|---|---|
| | O 1s | Al 2p | C 1s | Ag 3d | Pd 3d | |
| $Pd_5$ | 54.06 | 27.45 | 18.45 | 0.22 | 0.01 | 22 |
| $Pd_6$ | 53.96 | 29.41 | 16.38 | 0.24 | 0.01 | 24 |
| $Pd_{10}$ | 51.51 | 27.97 | 20.32 | 0.18 | 0.02 | 9 |

nanoparticles. In such AgPd catalytic systems, the Pd has typically been reported to be metallic, with Ag preferentially at the surface due to its lower surface cohesive energies.[21] XPS binding energies for the Ag $3d_{5/2}$ and Pd $3d_{5/2}$ peaks are 367.9 and 335.4 eV, respectively, with that of Ag being slightly lower than bulk Ag (368.3 eV) and the Pd slightly higher than its bulk equivalent (334.8 eV), which are likely due to the formation of AgO and the low particle size of the Pd (Figure S3).

## 2.2. Catalyst Testing

### *2.2.1. Catalyst Composition and Influence of Reactor Temperature*

The initial screening of the catalysts described in Table 1 was carried out at 100 °C and 10 bar with a gas composition of acetylene: ethene: hydrogen of 1:1:5 (total flow rate 140 mL $min^{-1}$, WHSV 84000 $cm^3\ h^{-1}\ g_{cat}{}^{-1}$). When the temperature of the reactor was set to 100 °C, both the $Pd_5$ and $Pd_6$ catalysts showed essentially no activity with maximum conversions seen of 6% and 11%, respectively. The $Pd_{10}$ catalyst was active at 100 °C, with an acetylene conversion above 90 % for 108 mins (Figure 3a). After this time, the catalyst activity decreased rapidly, and the conversion was less than 10 % after 148 min. The average selectivity to ethene and ethane was 66 % and 5 % respectively over the first 108 min and the selectivity to $C_4$ products was *ca*. 13 %. The rapid deactivation is likely to be due to the accumulation of oligomeric products on the catalyst surface. The reaction temperature is initially higher than the set temperature, 180 to 100 °C respectively, however, this decreases continuously and when below 150 °C the catalyst deactivation is rapid. We consider that this is due to high-boiling oligomers blocking the active sites, which can be reduced above this temperature.

When the reaction temperature was increased to 150 °C, catalytic activity of above 80% conversion over $Pd_5$ was observed for approximately 20 min and over $Pd_6$ this was modestly improved to approximately 40 min (Figure 3b,c). The maximum conversion was *ca*. 90% for both catalysts, and the selectivity to ethene was between 50%–60 % as the catalysts deactivated. Therefore, a minimal level of palladium is required to allow for reasonable acetylene hydrogenation activity beyond 1 h on-stream. In the case where the Pd content was high ($Pd_{95}Ag_5$), activity was high for a longer time on-stream (high conversion for *ca*. 300 min) but the selectivity to ethane was 100%, which concurs with previously reported results.[12b] Therefore, catalysts with Pd content above 20% were not considered to be effective for high ethene selectivity.

The $Pd_{10}$ catalyst, even with only a small increase in palladium proportion compared to $Pd_6$, maintained catalytic activity above 90% conversion for approximately 140 min before rapidly deactivating (Figure 3d). Over the $Pd_{10}$ catalyst full conversion of acetylene was achieved, with an average selectivity to ethene of *ca*. 70% and a selectivity to ethane of *ca*. 5%. The selectivity

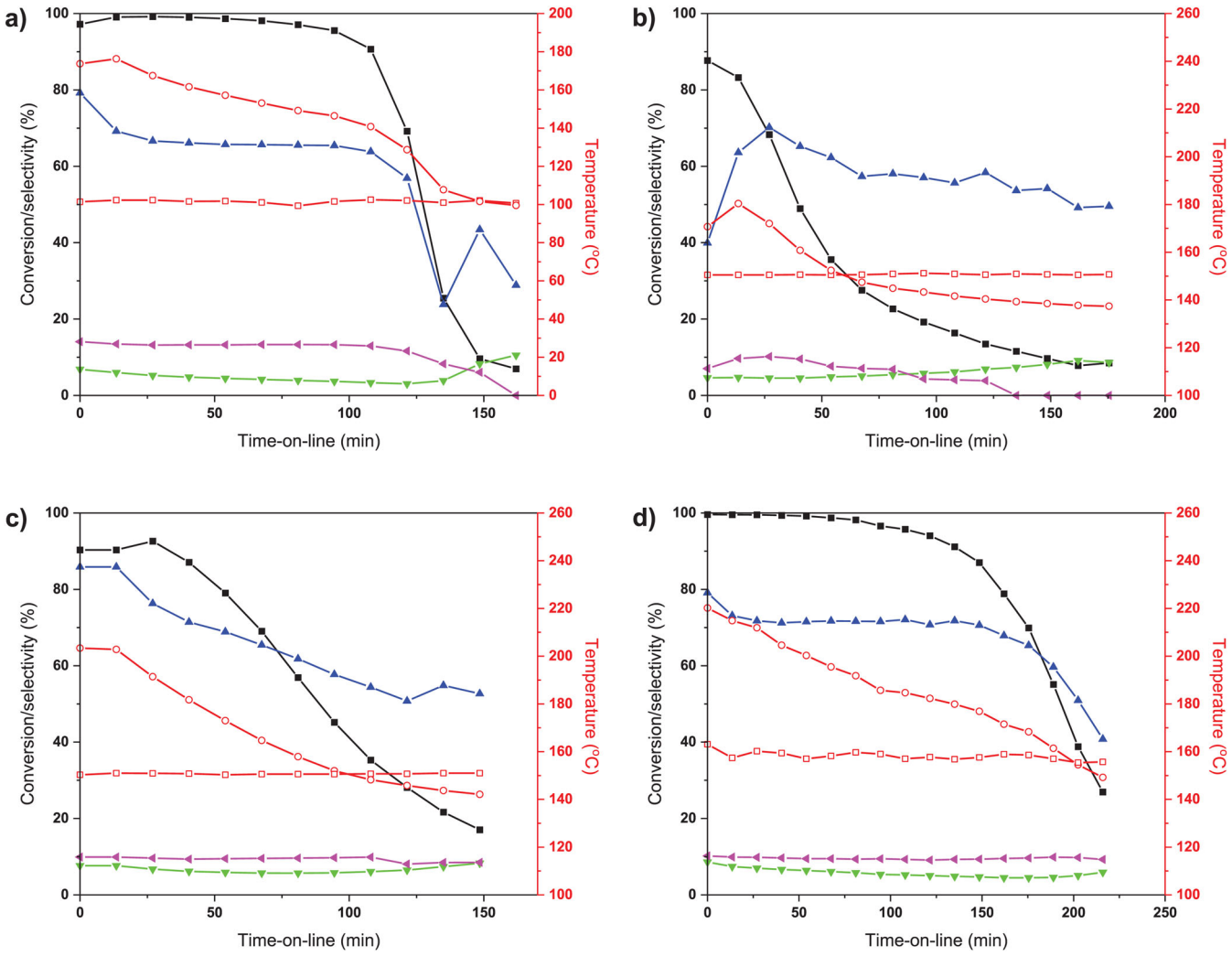


**Figure 3.** Comparison of the acetylene hydrogenation reaction profiles over three PdAg catalysts; $Pd_{10}$ at 100 °C (a), $Pd_5$ at 150 °C (b), $Pd_6$ at 150 °C (c), and $Pd_{10}$ at 150 °C (d). Selectivity to ethane (▼), ethene (▲) and $C_{4+}$ (◀); conversion of acetylene (■); reactor temperature (□) and catalyst bed temperature (°). Reaction conditions: Pressure 10 bar, 0.1 g Catalyst diluted in 3 g SiC, Acetylene 20 mL $min^{-1}$, ethene 20 mL $min^{-1}$, and hydrogen 100 mL $min^{-1}$.

to $C_4$ compounds was 10 %, which combined with the carbon balance of 93%–95% suggests that oligomers and high-boiling green oil derivatives were formed, which might block active sites, explaining the severe deactivation phenomena observed with time on-stream.

The hydrogenation steps of acetylene to ethene and ethene to ethane are highly exothermic (−174.6 and −136.9 kJ $mol^{-1}$, respectively[9]) and hence the set temperature of the reactor heating does not represent the actual catalyst bed temperature over an active catalyst. The data contained in Table 3 demonstrates this phenomenon, which is appreciable over the $Pd_{10}$ catalyst, for which the catalyst bed temperature increased to 170 °C when the external heating set temperature was 100 °C. For the $Pd_5$ and $Pd_6$ catalysts at 100 °C, the measured temperature was approximately 100 °C, implying that there was low activity. When the reactor was set to 150 °C, the measured temperature when using the $Pd_{10}$ catalyst was 220 °C. This is a large increase and may facilitate desorption of high-boiling oligomers from the catalyst surface and avoid site blocking and deactivation. The carbon mass balance (CMB) of the initial 40 min of the reactions can be seen in Table 3 and supports this inference. When the reactor temperature was set at 150 °C, the CMB varies according to the actual catalyst temperature. For example, over the lowest activity catalyst $Pd_5$, the average catalyst bed temperature was calculated to be 171 °C and the CMB was 89.4%. However, over more active catalysts such as $Pd_{10}$, the catalyst bed temperature was initially over 210 °C, such that the reactor thermocouple recorded an average temperature of 160 °C; in this case the CMB was increased to *ca.* 96%. Higher temperatures seem to disfavor oligomerization processes, and this might be linked to a faster desorption of important oligomerization precursors like butadiene at higher temperatures.

For comparison to sol-immobilization, Pd-Ag catalysts supported on alumina were also prepared by two other synthesis methods. Both catalysts comprised of a Pd-Ag ratio of 1:9, which is close to that of the sol-immobilized $Pd_{10}$ catalyst, however, one was prepared via a mechanochemical (MC) method and the second by a wet impregnation (WI) technique. Both were supported on a mechanochemically synthesized high surface area $\alpha$-$Al_2O_3$.[22] The catalysts were reacted at 150 °C and showed

**Table 3.** Comparison of reaction temperature and catalyst bed temperature to carbon mass balance under reaction conditions from average data measured over initial 45 min of reaction.

| Catalyst | 100 °C | | | 150 °C | | |
|---|---|---|---|---|---|---|
| | Reactor T (°C) | Catalyst T (°C) | CMB[a] (%) | Reactor T (°C) | Catalyst T (°C) | CMB (%) |
| $Pd_5$ | 101.6 | 97.1 | 99.3 | 150.5 | 171.0 | 89.4 |
| $Pd_6$ | 103.9 | 103.3 | 93.9 | 150.8 | 194.8 | 96.5 |
| $Pd_{10}$ | 101.5 | 143.3 | 94.8 | 160.0 | 212.9 | 95.5 |

[a] CMB carbon mass balance (calculation in methods section).

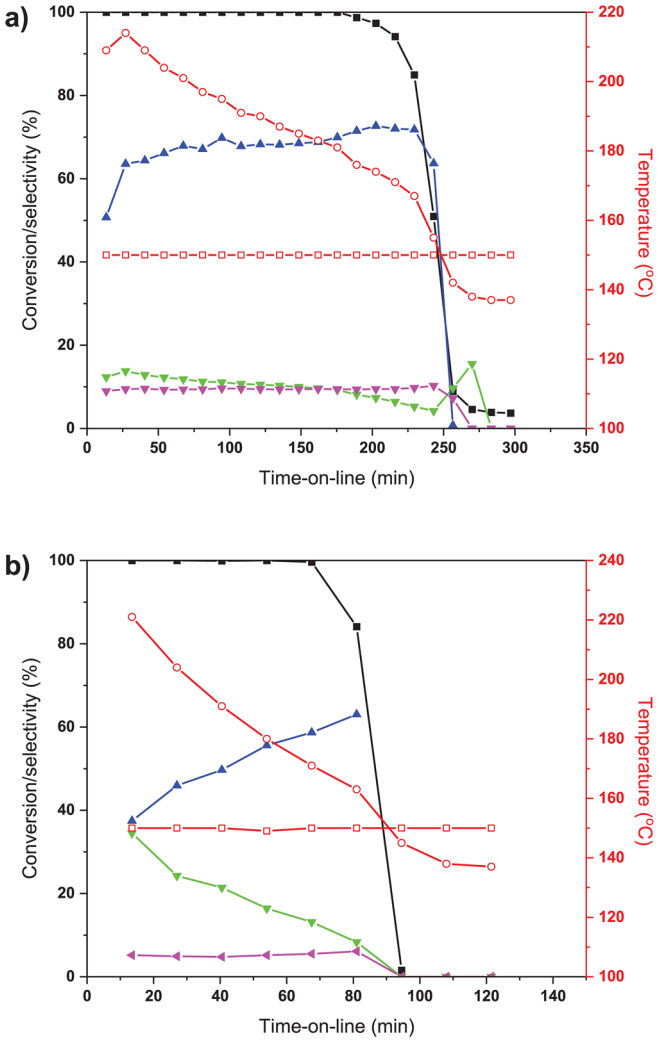


**Figure 4.** Acetylene hydrogenation reaction profiles over PdAg catalysts; 1 wt.% PdAg(1:9)/HSA-$\alpha$-$Al_2O_3$ (MC) (a) and 1 wt.% PdAg(1:9)/HSA-$\alpha$-$Al_2O_3$ (WI) at 150 °C (b). Selectivity to ethane (▼), ethene (▲) and C4+ (◀); conversion of acetylene (■); reactor temperature (□) and catalyst bed temperature (°). Reaction conditions: pressure 10 bar, temperature 150 °C, 0.1 g catalyst diluted in 3 g SiC, acetylene 20 mL $min^{-1}$, ethene 20 mL $min^{-1}$, and hydrogen 100 mL $min^{-1}$.

differing catalyst lifetimes and ethene selectivities (Figure 4). The shortest lifetime was seen over the WI catalyst, for which the acetylene conversion decreased rapidly after just 60 min TOL; here the ethene selectivity improved over the reaction period reaching *ca*. 60% before the catalyst deactivated. Over the MC

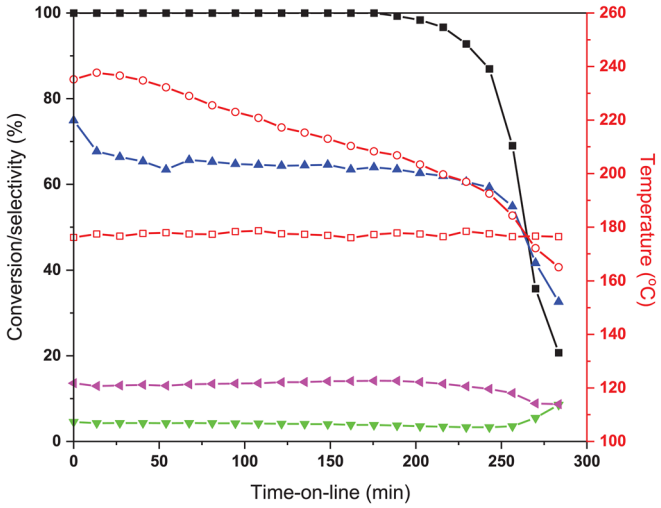


**Figure 5.** Time-on-line reaction profile of acetylene hydrogenation at 175 °C, over $Pd_{10}$. Selectivity to ethane (▼), ethene (▲) and $C4^+$ (◀); conversion of acetylene (■); reactor temperature (□), and catalyst bed temperature (°). Reaction conditions: pressure 10 bar, temperature 175 °C, 0.1 g catalyst diluted in 3 g SiC, acetylene 20 mL $min^{-1}$, ethene 20 mL $min^{-1}$, and hydrogen 100 mL $min^{-1}$.

catalyst, 100% acetylene conversion was achieved for over 200 min and the ethene selectivity modestly improved from 63% to 70% during this time. In both cases the catalyst bed temperature was greater than 200 °C for the first 20 min TOL, which is similar to that over the $Pd_{10}$ catalyst (Figure 3d). Over the MC catalyst the selectivity to ethane and $C_{4+}$ products were ca. 10%, similar to that over $Pd_{10}$; however, over the sol-immobilized catalyst the ethane selectivity was *ca*. 5 %. As previously reported, it can be assumed that the stability of the WI and MC catalysts on stream is rather related to the higher surface area of the $\alpha$-$Al_sO_3$ support offering more space for high-boiling oligomers, than to potential sintering phenomena.[4]

To probe the reaction temperature effect further, reactions were carried out over the $Pd_{10}$ catalyst at 175 °C (Figure 5). Great care was taken to assess the risks of increasing the temperature beyond 150 °C. The temperature safety ratings for the reactor and all internal pieces were considered as well as predicting the maximum temperature of the exotherm using other data and the exotherm data seen from lower temperatures with $Pd_{10}$. The reactor and computer had fail-safes should the temperature increase too much, and these were set at 260 °C, which was 10 °C higher than the predicted maximum temperature. The reactor

and the conditions were constantly monitored remotely for the first hour.

At 175 °C, the acetylene conversion over the $Pd_{10}$ catalyst was 100% for 176 min and over 90% for 235 min (Figure 5). The respective average selectivity over the first 175 min to ethene and ethane was approximately 65% and 4% and the average selectivity to $C_4$ components was *ca*. 13%. The exothermicity of the reaction caused the reactor to reach 238 °C which was lower than the predicted 250 °C.

By increasing the temperature to 175 °C the catalyst operational lifetime was increased likely due to desorption of oligomers formed on the catalyst, although this was at a cost to the selectivity of ethene which decreased from 71% at 150 °C to 65% when the temperature was set to 175 °C. However, this selectivity value was consistent over 200 min TOL. The selectivity of ethane was slightly reduced from 6.1% at 150 °C to 4.2% at 175 °C, however, the selectivity to $C_{4+}$ increased from 9.4 to 13.6%. The carbon mass balance over the first 45 min of the reaction during the period of the highest ethene selectivity was calculated to be 93.0% and decreased to an average of 90.7% above 200 min time-on-line when the catalyst bed temperature decreased below 200 °C and the ethene selectivity decreased to <60 %. The slightly increased selectivity to $C_{4+}$ products suggests that they are desorbed prior to oligomerizing, maintaining the relatively high CMB and catalyst lifetime when the catalyst bed temperature is maintained above 210 °C. The measured increase of short, volatile $C_{4+}$ molecules, which we use as evidence of reduced build-up of higher oligomers as seen in Figure 3d and Figure 5 over $Pd_{10}$ at 150 °C and 175 °C respectively. $C_{4+}$, particularly 1,3-butadiene are believed to be important precursors for the formation of higher non-volatile oligomers with acetylene. Therefore, an increased desorption at higher temperatures is commensurate with a reduced formation of the resulting higher oligomers.

The post-reaction samples were separated from the SiC diluent and any quartz wool used to form the catalyst bed and analyzed by electron microscopy to assess if the Ag-Pd nanoparticles had changed during the reaction period (Figures S4 and S5). Analysis of the sample tested at 150 °C and 175 °C revealed segregation of Pd had occurred (Figure 6). For the sample tested at 150 °C this segregation is modest and is primarily within the nanoparticles (Figure 6 and Figure S6). The ECD of the particles increased from 5.6 ± 3.3 to 6.1 ± 4.5 nm (164 particles sampled) as illustrated in Figure S4. In contrast, the segregation of Pd on the sample tested at 175 °C is greater and has resulted in the formation of separate Pd nanoparticles (Figure 6 and Figure S7), although these appear to be located near larger bimetallic particles, as highlighted. The morphology, size and composition have changed modestly for both used samples (Figure 6) although not to a significant extent, the ECD of the sample tested at 175 °C increased to 7.1 ± 3.4 nm (150 particles sampled) (Figures S4 and S5). The Ag content of nanoparticles measured by EDX mapping have increased by *ca*. 1%, however, over the sample size this is within the standard deviation error.

In addition to site blocking through oligomer build up, the segregation of Pd is not considered to contribute to deactivation. High Pd content catalysts such as 1 wt.% $Pd95Ag5/TiO_2$ over-hydrogenated acetylene and ethene streams resulting in 100% selectivity of ethane without any $C_{4+}$ produced, with a relatively long runtime (> 95% conversion) of 300 min. The testing data from Figures 3d and 5 show relatively stable selectivity to ethane and below 10%, therefore, the Pd segregation may have occurred when the catalyst bed was at the highest temperature (>210 °C), within the initial 30 min TOL. However, this is challenging to ascertain.

Reports detailing the influence of treatment conditions on the restructuring of Pt- or Pd-rich bimetallic catalysts suggest that Ag mobility is common.[11b,23] High temperature pre-reduction of the catalysts was shown to influence the formation of oligomers and hence enhance the ethene selectivity indirectly. In these cases, Ag was able to distribute over the Pd surface at reduction temperatures >400 °C. In the work reported here, the low Pd composition and the high exothermicity of the reaction may have facilitated Ag mobility whereby the Pd accumulates at the edges of the nanoparticles or causes segregation of Pd from the Ag-rich structure.[23a,24,25]

### 2.2.2. Varying the Feed-Stream Composition

To investigate how the acetylene and ethene concentrations affected the conversion and product selectivities, the gas flow rates were varied. Only $Pd_{10}$ was used in this testing as it was the most active catalyst studied. Initially the reaction mixture was changed so that it was no longer a competitive system, that is, acetylene or ethene hydrogenation. Following this, the acetylene:ethene flow rate ratio was decreased whilst keeping the same flow rate of hydrogen.

The noncompetitive acetylene or ethene-only hydrogenation experiments are illustrated in Figure 7. When ethene was removed from the feed-stream, acetylene conversion was above 90% for 135 min compared to the reaction with ethene where it was above 90% for 235 min. The lower runtime could be due to the total gas flow rate being lower and hence the residence time may be slightly longer. If the residence time is longer, more oligomers may form which would poison the catalyst. The carbon balance of the reaction was also lower when ethene was excluded. With ethene the carbon balance was 93%, whereas without ethene the carbon balance dropped to 85 %. This would support the inference that more oligomers are formed via acetylene.

The selectivity to ethene was improved when ethene was absent from the feed stream at 175 °C increasing from 65 % with ethene to over 70 % without ethene. The selectivity to ethane was approximately comparable, however the selectivity to $C_{4+}$ products was lower when ethene was removed decreasing from ca. 15 % with ethene to 10 % without ethene. It has already been reported elsewhere that ethene might take part in oligomerization processes of acetylene-derived intermediates during selective hydrogenation on Pd surfaces.[26]

When ethene is fed into the reactor without acetylene present, the conversion of ethene was below 20% however, this increases to 60% at 250 min TOL (Figure 7b). The selectivity to ethane is consistently above 80% though interestingly, no $C_{4+}$ products were detected, which suggests that the $C_4$ products

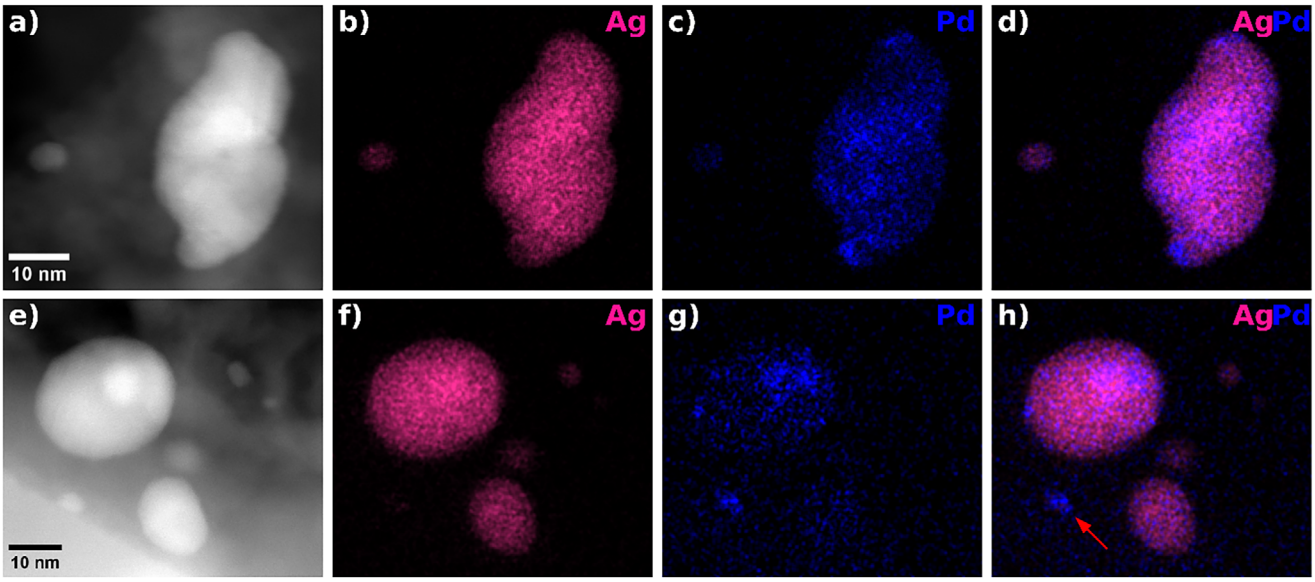


**Figure 6.** (a) HAADF-STEM image of AgPd nanoparticles of $Pd_{10}$ tested at (a) 150 °C and (e) at 175 °C, associated with STEM-EDX elemental maps of (b and f) Ag, (c and g) Pd, (d and h) overlaid Ag and Pd maps Arrow indicates presence of high Pd content nanoparticle.

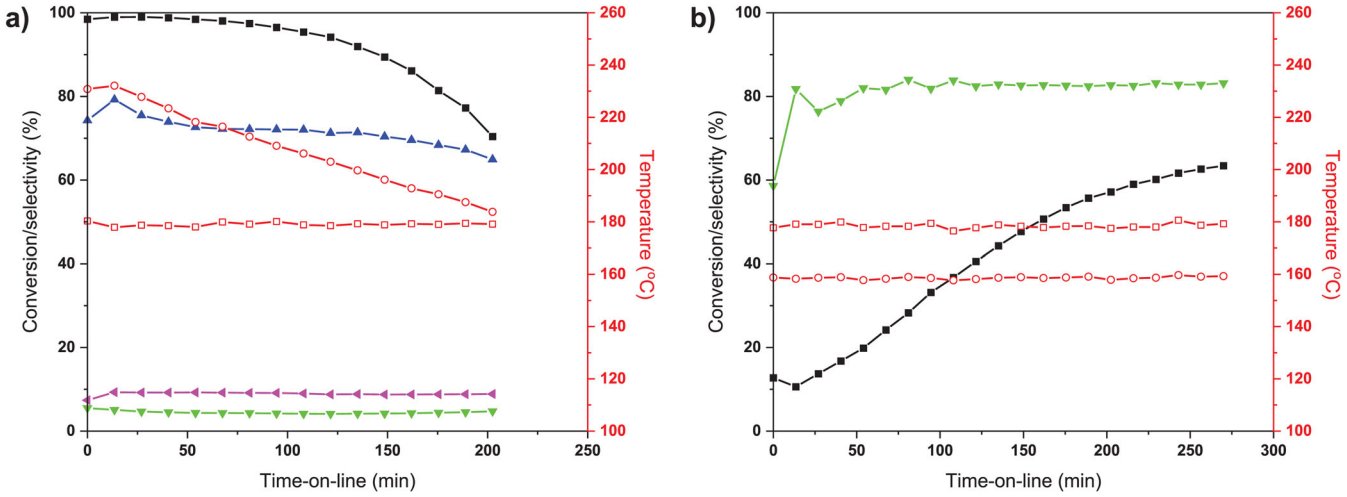


**Figure 7.** Time-on-line catalytic reaction profiles over $Pd_{10}$ where acetylene only (a) or ethene only (b) were used in the feedstock. Selectivity to ethane (▼), ethene (▲) and C4+ (◀); conversion of acetylene (■); reactor temperature (□) and catalyst bed temperature (°). Reaction conditions: pressure 10 bar, temperature 175 °C, 0.1 g catalyst diluted in 3 g SiC, acetylene 20 mL $min^{-1}$ or ethene 20 mL $min^{-1}$, and hydrogen 100 mL $min^{-1}$.

come from the acetylene or acetylene-derived surface intermediates. The reactor temperature was also lower than the set temperature by about 15 °C, which is due to the lower exothermicity of only the second step and the overall lower flow of unsaturated hydrocarbons.

The carbon balance for the reaction was *ca*. 95% for the first 100 min and decreased to 90% over the next 170 min. Because no $C_{4+}$ products were detected, it is not clear where the carbon is lost to. Potentially, under these conditions ethene may have formed $>C_{4+}$ products and it would be expected that these longer chains would have eventually deactivated the catalyst.

As the acetylene flow rate is decreased from 20 ml $min^{-1}$ (Figure 5) to 10 and 5 mL $min^{-1}$ (Figure 8), three different effects can be observed; first, the catalyst lifetime was increased, second the selectivity to ethene decreases, and finally selectivity to ethane increases whilst selectivity to $C_{4+}$ products decreases. The selectivity of ethene decreasing can be rationalized through fewer active sites being used by acetylene, therefore more ethene can adsorb and react. We note that the total WHSV has slightly changed as the $H_2$ flow rate was not increased to compensate for the reduced acetylene feed. However, the change in residence time is not considered to be significant enough to increase operational lifetime as observed. As seen in the non-competitive ethene hydrogenation (Figure 7b), no $C_{4+}$ products were detected when hydrogenating ethene. As the relative concentration of acetylene decreases, less $C_{4+}$ products would be formed which would mean less oligomers are poisoning the catalyst. This would have the effect of increasing the runtime as supported by the reaction profiles (Figure 8).

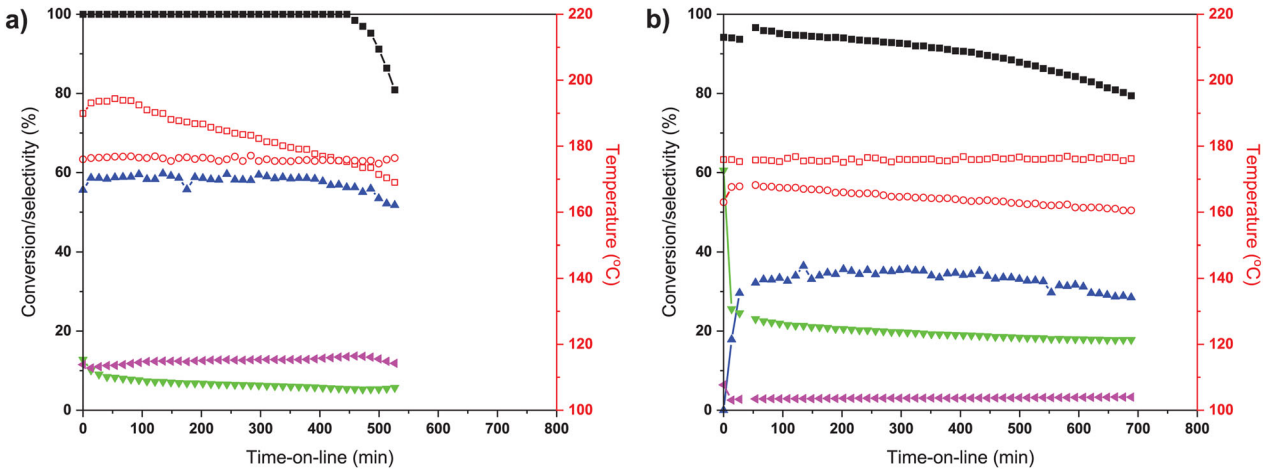


**Figure 8.** Time-on-line catalytic reaction profiles over $Pd_{10}$ where acetylene: ethene ratios of (a) 0.5:1 and (b) 0.25:1 were used. Selectivity to ethane (▼), ethene (▲) and $C_{4+}$ (◀); conversion of acetylene (■); reactor temperature (□) and catalyst bed temperature (°). Reaction conditions: pressure 10 bar, temperature 175 °C, 0.1 g catalyst diluted in 3 g SiC, acetylene 5–10 mL $min^{-1}$ and ethene 20 mL $min^{-1}$, and hydrogen 100 mL $min^{-1}$.

Interestingly, with the reaction using a 0.25:1 acetylene: ethene gas feed (Figure 8b) the catalyst lifetime is extended further, typically when the catalysts start to deactivate, they deactivate quickly as seen in Figures 3 and 4. In this experiment the conversion does not reach 100% and the catalyst appears to be deactivating slowly from the start of the reaction. Given the significantly lower acetylene feed concentration it can be assumed that the formation rate of high-boiling oligomers is decreased explaining slower deactivation. This extended catalyst lifetime was noteworthy, even if the selectivity to ethene and ethane was poor at about 35% and 20%, respectively. We consider that the low acetylene concentration results in a reaction profile comparable to that of using ethene only in the feedstream (Figure 7b). In this reaction the catalyst bed temperature was lower than the reactor set temperature, and a low selectivity to $C_{4+}$ products can be observed as a consequence of lower oligomer formation as seen with the feed ratio of 0.5:1 (Figure 8a), resulting in the extended catalyst lifetime.

## 3. Conclusions

In this study Pd-Ag alloyed nanoparticles of various compositions supported on transitional alumina were prepared by a sol-immobilization technique and compared with materials synthesized on high surface area alpha-alumina via a ball milling and a more conventional wet-impregnation procedure. Despite the significantly smaller surface area of the transitional alumina support, Pd-Ag nanoparticles were in all three cases between 7–9 nm, underlining the strength of the sol-immobilization technique for particle size control during synthesis. To assess catalytic properties under particularly challenging conditions the materials were tested in the selective hydrogenation of equally concentrated acetylene-ethene mixtures mimicking the effluent stream of a hypothetical methane-to-ethene conversion plant. Catalytic activity and ethene selectivity were highly dependent on the Pd concentration of the catalyst. While Ag most likely dilutes active Pd sites, it increases selectivity to ethene but decreases catalytic activity. A molar composition of 10% Pd and 90% Ag in the nanoparticles was identified as the optimum. Increasing the reaction temperature from 100 to 150 °C enhanced average ethene selectivity (up to 71 %) and lifetime (up to 140 min) over $Pd_{10}Ag_{90}$ under the chosen reaction conditions by presumably facilitating desorption of otherwise active site blocking acetylene oligomers. Further increase in reaction temperature to 175 °C resulted in increased catalyst lifetime to the detriment of ethene selectivity while favoring the oligomerization processes. Average ethene selectivity on-line over the sol-immobilized $Pd_{10}Ag_{90}$ catalyst (71%) outperformed the wet-impregnated (51%) and the mechanochemically synthesized counterparts (67%) at 150 °C. Despite the much lower surface area of the transitional alumina support, the sol-immobilized catalyst demonstrates higher stability on-line (*ca.* 140 min) than the conventional wet-impregnated material (*ca.* 60 min). Post reaction analysis supports the inference that active site blocking high boiling oligomers are more likely to cause deactivation than particle sintering or Pd dissolution. Investigating the role of acetylene and ethene in the formation of oligomers by variation of the feed gas composition suggests that important oligomerization precursors are solely formed in the presence of acetylene. Nevertheless, it is very likely that not only acetylene but also ethene further react with those precursors to high-boiling hydrocarbons. Better understanding the origin and mechanism of oligomer formation in equally concentrated acetylene-ethene mixtures might pave the way to the development of synthesis procedures of even better performing materials under such challenging reaction conditions.

## 4. Experimental Section

### 4.1. Catalyst Preparation

#### *4.1.1. Sol-Immobilization*

Catalysts were prepared by a sol-immobilization method; silver nitrate ($Ag(NO_3) \geq 99.9995\%$, Thermo–Fisher Scientific), and palladium nitrate ($Pd(NO_3)_2 \bullet 2H_2O$ (*ca.* 40% Pd basis, Merck) were

dissolved separately in deionized water to form solutions with a metal concentration of 5 mg $mL^{-1}$. The containers with solution were wrapped in aluminum foil and stirred overnight and used within 3 days to avoid oxidation. A solution of polyvinyl alcohol (9000–10,000 Da, 80% hydrolyzed, Merck) was also prepared with a concentration of 10 mg $mL^{-1}$. For 2 g of a 1 wt.% catalyst, the amount of dissolved metal required, accounting for the total metal composition, was added to deionized water (800 mL). Polyvinyl alcohol was then added so that the weight ratio of PVA:metal was 1.2. A solution of sodium borohydride (0.1 mol $dm^{-3}$) was added quickly ($NaBH_4$:metal molar ratio = 5). After 30 min of stirring, the ground $Al_2O_3$ support (1.98 g, Saint-Gobain NorPro, experimental alumina carrier no. 750,088) was then added to the solution with 8 drops of concentrated sulphuric acid to lower the pH to 1–2. This suspension was stirred for a further hour, after which the suspension was washed with deionized water (2000 mL), filtered, and then dried in an oven (110 °C, 16 h). The resultant Ag-Pd/$Al_2O_3$ catalysts were then denoted as $Pd_x$, where $x$ represents the % composition with Ag as measured with ICP-MS.

#### 4.1.2. Mechanochemical

For the synthesis of high surface area $\alpha$-$Al_2O_3$ (HSA-$\alpha$-$Al_2O_3$), 1 g of $\gamma$-AlOOH was ball milled in a Fritsch planetary micro mill Pulverisette P7 (classic line, all milling equipment made of zirconia, 45 mL milling jar) together with three grinding balls (d. 15 mm) at 450 rpm for 6 h (24 cycles of 15 min milling with a 5 min cooling break in-between). The obtained high surface area $\alpha$-$Al_2O_3$ revealed a BET surface area of 110 $m^2$ $g^{-1}$ via $N_2$ physisorption. Further details on the synthesis procedure and material properties can be found in previously published studies.[4,22] For the deposition of $Pd_1Ag_9$ nanoparticles, palladium and silver were added in a molar ratio of 1 to 9 in an amount corresponding to a total metal loading of 5 wt.% to 950 mg of $\gamma$-AlOOH. The mixture was milled for 6 h (24 cycles of 15 min with a 5 min cooling break in-between) at 500 rpm in the presence of three grinding balls (d. 15 mm). 200 mg of the obtained 5 wt.% $Pd_1Ag_9$/HSA-$\alpha$-$Al_2O_3$ material was further diluted with 800 mg freshly prepared HSA-$\alpha$-$Al_2O_3$ by ball milling at 450 rpm for 1 h (4 cycles of 15 min with a 5 min cooling break in-between) with three grinding balls (d. 15 mm). The obtained material was furthermore activated in pure hydrogen gas flow (100 mL $min^{-1}$) at 150 °C (2 °C $min^{-1}$) for 3 h and annealed under pure argon flow (100 mL $min^{-1}$) at 600 °C (5 °C $min^{-1}$) for 10 h in a tubular oven for comparison. The final 1 wt.% $Pd_1Ag_9$/HSA-$\alpha$-$Al_2O_3$ catalyst is according to the synthesis procedure denoted as MC in the following.

#### 4.1.3. Wet Impregnation

Palladium(II) nitrate and silver(I) nitrate were dissolved in deionized water (50 mL) in a molar ratio of 1 to 9 to yield a total metal loading of 1 wt.% in the final material. Freshly prepared HSA-$\alpha$-$Al_2O_3$ (1.98 g) was added as support material and the mixture was stirred for 1 h at room temperature. The resulting slurry was dried under reduced pressure in a rotary evaporator (2 h, 70 °C). The recovered wet powder was further dried at 75 °C overnight and calcined at 120 °C for 2 h. The obtained material was furthermore reduced in pure hydrogen gas flow (100 mL $min^{-1}$) at 150 °C (2 °C $min^{-1}$) for 3 h and annealed under pure argon flow (100 mL $min^{-1}$) at 600 °C (5 °C $min^{-1}$) for 10 h in a tubular oven. The final 1 wt.% $Pd_1Ag_9$/HSA-$\alpha$-$Al_2O_3$ catalyst is according to the synthesis procedure denoted as WI in the following.

### 4.2. Catalyst Testing

Selective hydrogenation of acetylene was carried out in a specially adapted reactor setup at the Max-Planck-Institut für Kohlenforschung (Mülheim an der Ruhr, Germany) (Figure S8). Due to the inherent risk of explosion associated with pressurized acetylene, several safety features were considered in the fully remotely controllable reactor setup situated in an explosion safe cubicle. Further details on the reactor setup can be found in other published studies of the Schüth group.[4a,14,24] Catalytic testing was carried out in a plug-flow fixed bed reactor (steel, 8 mm i.d.) under pressure of 10 bar in a temperature range from 100 to 175 °C. The reactor was equipped with an external oven and a thermocouple for heat control. The temperature inside the reactor was measured on-stream via a second thermocouple immersed in the catalyst bed. Hydrogen, nitrogen, ethene and methane were purchased from Air Liquide and used without any further purification. Acetylene (Air Liquide) was passed over a bed of previously dried zeolite A and alumina extrudates to remove acetone and other impurities prior to use and then compressed to 25 bar. Flow of gases was controlled individually via previously calibrated mass flow controllers to WHSV between 84000 and 99000 $cm^3$ $h^{-1}$ $g_{cat}{}^{-1}$. 100 mg of pelletized, crushed and sieved catalyst (300–400 µm) was physically mixed with 3 g silicon carbide and placed onto a metal sieve inside the reactor tube. Quartz wool was added on top to hold the catalyst bed in place. All tubes downstream of the reactor were heated above 150 °C to avoid product condensation. A constant flow of methane (10 mL $min^{-1}$) was added after the reactor to the product or bypassed feed gas stream as internal standard. The composition of the feed and product gas stream was analyzed via an online gas chromatograph (Agilent 7890B). Detection of ethane, ethene, acetylene, $C_3$ (propane, propylene) and $C_4$ (butane, 1-butene) was done via three sequential columns and corresponding detectors; a Rxi-5Sil MS column (Restek) with a flame ionization detector (FID) to separate long chain hydrocarbons, a RT-alumina BOND/$Na_2SO_4$ column (Restek) with FID to separate hydrocarbons up to $C_4$ and a RT-Msieve 5A column (Restek) with thermal conductivity detector (TCD) to detect and analyze inert gases. Flows of respective compounds were calculated via the peak area ratio to methane using previously assessed response factors. Acetylene (and ethene) conversion and selectivity to detected compounds was calculated according to the following equations using molar flows $\dot{n}$.

$$\text{Conversion}\ (\%) = 100 \times \frac{\dot{n}_{C_2H_2.out}}{\dot{n}_{C_2H_2.in}} \quad (1)$$

$$\text{Selectivity}_{C_2H_4}\ (\%) = 100 \times \frac{\dot{n}_{C_2H_4.out} - \dot{n}_{C_2H_4.in}}{\dot{n}_{C_2H_2.in} - \dot{n}_{C_2H_2.out}} \quad (2)$$

$$\text{Selectivity}_{C_2H_6}\ (\%) = 100 \times \frac{\dot{n}_{C_2H_6.out}}{\dot{n}_{C_2H_2.in} - \dot{n}_{C_2H_2.out}} \quad (3)$$

$$\text{Selectivity}_{C_3}\ (\%) = 100 \times \frac{\dot{n}_{C_3.out} \cdot 1.5}{\dot{n}_{C_2H_2.in} - \dot{n}_{C_2H_2.out}} \quad (4)$$

$$\text{Selectivity}_{C_4}\ (\%) = 100 \times \frac{\dot{n}_{C_4.out} \cdot 2}{\dot{n}_{C_2H_2.in} - \dot{n}_{C_2H_2.out}} \quad (5)$$

$$\text{Carbon Balance}\ (\%) = 100 \times \frac{\dot{n}_{C_2H_2.out} + \dot{n}_{C_2H_4.out} + \dot{n}_{C_2H_6.out} + \dot{n}_{C_3.out} \cdot 1.5 + \dot{n}_{C_4.out} \cdot 2}{\dot{n}_{C_2H_2.in} + \dot{n}_{C_2H_4.in}} \quad (6)$$

Runtime is the amount of time that the catalyst conversion was over a specified value. It is usually denoted as x min (conversion >95%).

### 4.3. Characterization

Inductively coupled plasma – Mass spectrometry (ICP-MS) was acquired by analytical services at Cardiff University, using an Agilent 7900 ICP-MS with IAS Autosampler. The ICP-MS was calibrated using Perkin Elmer Multi Element Cal 4 (Pd) and Cal 3 (Ag) at 0, 1, 10, 100, 1000 μg $L^{-1}$ as well as using an internal standard Agilent ICP-MS IS Mix 5188–6525 (72Ge). To prepare samples for ICP-MS, a known mass of catalyst was digested using nitric acid (1 mL, 70%). After digesting overnight, the solutions were diluted up to 10 mL using deionized water and filtered with a Fisher brand™ 0.45 μm PTFE hydrophilic syringe filter to remove any solids.

Powder X-ray diffraction (XRD) analysis was performed on a PAN alytical X'Pert Pro diffractometer using a Ni-filtered Cu-K$\alpha$ radiation source operating at 40 KV and 40 mA. Diffraction patterns were recorded between 5°–80° 2$\theta$ at a step size of 0.0167° (resulting in a total run time of *ca*. 40 mins) using a back filled sample holder. Diffraction patterns were identified using the Inorganic Crystal Structure Database (ICSD) Powder Diffraction File.

X-ray photoelectron spectroscopy data acquisition and analysis was performed by Dr David Morgan in Cardiff University using a Thermo Fisher Scientific K-alpha + spectrometer. Samples were analyzed using a micro-focused monochromatic Al X-ray source (72 W) using the "400-μm spot" mode, which provided an analysis defining elliptical x-ray spot of ca. 400×600 μm. Data was recorded at pass energies of 150 eV for survey scans and 40 eV for high resolution scan with 1 eV and 0.1 eV step sizes respectively. Charge neutralization of the sample was achieved using a combination of both low energy electrons and argon ions.

Data analysis was performed in CasaXPS v2.3.26 rev1.1 N after calibrating the data to the lowest C(1s) component of adventitious carbon and taken to have a value of 284.8 eV or for alumina samples, to the Al 2p peak at 74.6 eV as this was found to be more stable a reference for these samples. Quantification was made using a Shirley type background and Scofield sensitivity factors, with an electron energy dependence according to the TPP-2 M equation.

Transmission electron microscopy (TEM) was performed on a JEOL JEM-2100 operating at 200 kV. Samples were prepared by drop-casting over 300 mesh copper grids coated with holey carbon film. Scanning transmission electron microscopy (STEM) was performed using a Thermo-Scientific Spectra 200 Scanning Transmission Electron Microscope, at an accelerating voltage of 200 kV and with a convergence semi-angle of 30 mrad. The HAADF detector had an inner collection angle of approximately 56 mrad (outer angle of approximately 200 mrad). EDX spectrum images were acquired on a Super-X detector. Particle diameters were measured manually, taking measurements by outlining the respective particle and calculating the equivalent circular diameter in the Particle Spy Python package (ref https://zenodo.org/records/5094360). When analyzing the signals from a bimetallic catalyst, further steps must be taken to separate the signals from palladium and silver as their L$\alpha$ characteristic X-ray signals are seen at 2.838 and 2.984 keV, respectively. Because of this similarity, Pd and Ag signals can be mistaken for each other which would give a false map. The maps for the bimetallic catalysts were processed using Thermo Scientific Velox Software, which allowed for the signals to be separated with a high degree of certainty.

## Acknowledgements

We thank the Max Planck Society and the Cardiff University for financial support to create the FUNCAT Centre. We are grateful to the fine mechanic workshop (led by Dirk Ullner) and the technical laboratories (led by Niels Theyssen) at the Max-Planck-Institut für Kohlenforschung for the support in the maintenance of the reactor setup and its sophisticated safety structure. We wish to acknowledge the use of the EPSRC funded Physical Sciences, Data-science Service hosted by the University of Southampton and STFC under grant number EP/S020357/1. Jonathan M. Mauß is thankful for a Kekulé scholarship by Fonds der Chemischen Industrie (FCI). We thank the CCI Electron Microscopy Facility which has been part funded by the European Regional Development Fund through the Welsh European Funding Office and The Wolfson Foundation. Open Access funding provided by the Max-Planck Society. The authors thank the analytical services in Cardiff University for assistance with ICP-MS analysis. Jake O. Williams thanks the Royal Society of Chemistry for funding under the "Researcher Development Grant" scheme (D22-0935807625).

## Conflict of Interests

The authors declare no conflict of interest.

## Data Availability Statement

The data that support the findings of this study are available in the supplementary material of this article.

**Keywords:** Acetylene · AgPd nanoparticles · Ethene · Hydrogenation · Sol immobilization

[1] H. Zimmermann, R. Walzl, in *Ullmann's Encyclopedia of Industrial Chemistry*, John Wiley & Sons Ltd, Weinheim **2009**.
[2] Ethylene production capacity globally 2022, https://www.statista.com/statistics/1067372/global-ethylene-production-capacity (accessed: June 2024).
[3] A. Makarov, V. Kulagin, T. Mitrova, *Global Russian Energy Outlook* **2019**, *36*, 1430–1435.
[4] a) K. S. Kley, J. D. Bellis, F. Schüth, *Catal. Sci. Technol.* **2023**, *13*, 119–131; b) E. Delikonstantis, E. Igos, M. Augustinus, E. Benetto, G. D. Stefanidis, *Sustainable Energy Fuels* **2020**, *4*, 1351–1362; c) E. Delikonstantis, M. Scapinello, G. D. Stefanidis, *Processes* **2019**, *7*, 68; d) B. Wang, H. M. Guan, *Catal. Lett.* **2016**, *146*, 2193–2199; e) E. Delikonstantis, M. Scapinello, G. D. Stefanidis, *Fuel Process. Technol.* **2018**, *176*, 33–42.
[5] a) P. Pässler, W. Hefner, K. Buckl, H. Meinass, A. Meiswinkel, H.-J. Wernicke, G. Ebersberg, R. Müller, J. Bässler, H. Behringer, D. Mayer, in *Ullmann's Encyclopedia of Industrial Chemistry*, John Wiley & Sons Ltd, Weinheim **2011**; b) I.-T. Trotuş, T. Zimmermann, F. Schüth, *Chem. Rev.* **2014**, *114*, 1761–1782.
[6] a) A. D. Benavidez, P. D. Burton, J. L. Nogales, A. R. Jenkins, S. A. Ivanov, J. T. Miller, A. M. Karim, A. K. Datye, *Appl. Catal., A* **2014**, *482*, 108–115; b) M. T. Ravanchi, S. Sahebdelfar, S. Komeili, *Rev. Chem. Eng.* **2018**, *34*, 215–237; c) L. A. Tyurina, S. A. Nikolaev, S. A. Gurevich, V. M. Kozhevin, V. V. Smirnov, K. L. Zanaveskin, *Catal. Industry* **2009**, *1*, 179–183.
[7] M. R. Ball, K. R. Rivera-Dones, E. B. Gilcher, S. F. Ausman, C. W. Hullfish, E. A. Lebrón, J. A. Dumesic, *ACS Catal.* **2020**, *10*, 8567–8581.
[8] G. Tiwari, G. Sharma, R. Verma, P. Gakhad, A. K. Singh, V. Polshettiwar, B. R. Jagirdar, *Chem. Eur. J.* **2023**, *29*, e202301932.
[9] J. H. Lee, S. K. Kim, I. Y. Ahn, W.-J. Kim, S. H. Moon, *Korean J. Chem. Eng.* **2012**, *29*, 169–172.
[10] G. Lee, W.-J. Jeong, H.-G. Ahn, *J. Nanosci. Nanotechnol.* **2020**, *20*, 5800–5803.
[11] a) A. A. Lamberov, S. R. Egorova, I. R. Il'yasov, K. K. Gil'manov, S. V. Trifonov, V. M. Shatilov, A. S. Ziyatdinov, *Kinet. Catal.* **2007**, *48*, 136–142; b) G. X. Pei, X. Y. Liu, A. Wang, A. F. Lee, M. A. Isaacs, L. Li, X. Pan, X.

Yang, X. Wang, Z. Tai, K. Wilson, T. Zhang, *ACS Catal.* **2015**, *5*, 3717–3725; c) Q. Zhang, J. Li, X. Liu, Q. Zhu, *Appl. Catal., A* **2000**, *197*, 221–228.
[12] a) L. Chen, X.-T. Li, S. Ma, Y.-F. Hu, C. Shang, Z.-P. Liu, *ACS Catal.* **2022**, *12*, 14872–14881; b) T. D. Shittu, O. B. Ayodele, *Front. Chem. Sci. Eng.* **2022**, *16*, 1031–1059; c) L. Zhang, M. Zhou, A. Wang, T. Zhang, *Chem. Rev.* **2020**, *120*, 683–733.
[13] E. Vignola, S. N. Steinmann, A. Al Farra, B. D. Vandegehuchte, D. Curulla, P. Sautet, *ACS Catal.* **2018**, *8*, 1662–1671.
[14] J. M. Mauß, F. Schüth, *ChemSusChem* **2024**, *18*, e202401593.
[15] D. R. Jones, S. Iqbal, P. J. Miedziak, D. J. Morgan, J. K. Edwards, Q. He, G. J. Hutchings, *Top. Catal.* **2018**, *61*, 833–843.
[16] P. R. Murthy, J.-C. Zhang, W.-Z. Li, *Catal. Sci. Technol.* **2021**, *11*, 3609–3618.
[17] Y. Liang, B. Zhao, Q. Tang, L. Liu, J. Dong, *Catal. Lett.* **2022**, *152*, 3489–3497.
[18] a) M. Brust, M. Walker, D. Bethell, D. J. Schiffrin, R. Whyman, *J. Chem. Soc., Chem. Commun.* **1994**, *7*, 801–802; b) A. Jouve, M. Stucchi, I. Barlocco, C. Evangelisti, F. Somodic, A. Villa, L. Prati, *Top. Catal.* **2018**, *61*, 1928–1938; c) A. Villa, D. Wang, G. M. Veith, F. Vindigni, L. Prati, *Catal. Sci. Technol.* **2013**, *3*, 3036–3041.
[19] a) R. Albilali, M. Douthwaite, Q. He, S. H. Taylor, *Catal. Sci. Technol.* **2018**, *8*, 252–267; b) V. Peneau, Q. He, G. Shaw, S. A. Kondrat, T. E. Davies, P. Miedziak, M. Forde, N. Dimitratos, C. J. Kiely, G. J. Hutchings, *Phys. Chem. Chem. Phys.* **2013**, *15*, 10636–10644.
[20] a) S. Cattaneo, D. Bonincontro, T. Bere, C. J. Kiely, G. J. Hutchings, N. Dimitratos, S. Albonetti, *ChemNanoMat* **2020**, *6*, 420–426; b) J. A. Lopez-Sanchez, N. Dimitratos, P. Miedziak, E. Ntainjua, J. K. Edwards, D. Morgan, A. F. Carley, R. Tiruvalam, C. J. Kiely, G. J. Hutchings, *Phys. Chem. Chem. Phys.* **2008**, *10*, 1921–1930; c) C. B. Paris, A. G. Howe, R. J. Lewis, D. Hewes, D. J. Morgan, Q. He, J. K. Edwards, *ACS Catal.* **2022**, *12*, 4440–4454.
[21] a) A. V. Ruban, H. L. Skriver, *Comput. Mater. Sci.* **1999**, *15*, 119–143; b) A. V. Ruban, H. L. Skriver, J. K. Nørskov, *Phys. Rev. B* **1999**, *59*, 15990–16000; c) L.-L. Wang, D. D. Johnson, *J. Am. Chem. Soc.* **2009**, *131*, 14023–14029.
[22] A. P. Amrute, Z. Łodziana, H. Schreyer, C. Weidenthaler, F. Schüth, *Science* **2019**, *366*, 485–489.
[23] a) Y. Jin, A. K. Datye, E. Rightor, R. Gulotty, W. Waterman, M. Smith, M. Holbrook, J. Maj, J. Blackson, *J. Catal.* **2001**, *203*, 292–306; b) S. Komeili, M. T. Ravanchi, A. Taeb, *Appl. Catal., A* **2015**, *502*, 287–296; c) J. Tang, L. Deng, H. Deng, S. Xiao, X. Zhang, W. Hu, *J. Phys. Chem. C* **2014**, *118*, 27850–27860; d) E. Vignola, S. N. Steinmann, K. Le Mapihan, B. D. Vandegehuchte, D. Curulla, P. Sautet, *J. Phys. Chem. C* **2018**, *122*, 15456–15463.
[24] H. Röder, R. Schuster, H. Brune, K. Kern, *Phys. Rev. Lett.* **1993**, *71*, 2086–2089.
[25] A. Christensen, A. V. Ruban, P. Stoltze, K. W. Jacobsen, H. L. Skriver, J. K. Nørskov, F. Besenbacher, *Phys. Rev. B* **1997**, *56*, 5822–5834.
[26] a) I.-T. Trotuş, *PhD Thesis*, Ruhr-Universität Bochum, Bochum **2016**; b) K. S. Kley, *PhD Thesis*, Ruhr-Universität Bochum, Bochum **2022**; c) Ö. Agbaba, I.-T. Trotuş, W. Schmidt, F. Schüth, *Ind. Eng. Chem. Res.* **2023**, *62*, 1819–1825; d) I.-T. Trotuş, T. Zimmermann, N. Duyckaerts, J. Geboers, F. Schüth, *Chem. Commun.* **2015**, *51*, 7124–7127.

Manuscript received: October 25, 2024
Revised manuscript received: January 30, 2025
Accepted manuscript online: March 3, 2025
Version of record online: April 10, 2025